



UNIVERSITY OF LEEDS

This is a repository copy of *Solvent-Mediated Enhancement of Additive-Controlled Crystallization*.

White Rose Research Online URL for this paper:

<https://eprints.whiterose.ac.uk/179439/>

Version: Supplemental Material

Article:

Nahi, O, Kulak, AN orcid.org/0000-0002-2798-9301, Broad, A et al. (6 more authors) (2021) Solvent-Mediated Enhancement of Additive-Controlled Crystallization. *Crystal Growth and Design*. ISSN 1528-7483

<https://doi.org/10.1021/acs.cgd.1c01002>

© 2021 American Chemical Society. This is an author produced version of an article published in *Crystal Growth and Design*. Uploaded in accordance with the publisher's self-archiving policy.

Reuse

Items deposited in White Rose Research Online are protected by copyright, with all rights reserved unless indicated otherwise. They may be downloaded and/or printed for private study, or other acts as permitted by national copyright laws. The publisher or other rights holders may allow further reproduction and re-use of the full text version. This is indicated by the licence information on the White Rose Research Online record for the item.

Takedown

If you consider content in White Rose Research Online to be in breach of UK law, please notify us by emailing eprints@whiterose.ac.uk including the URL of the record and the reason for the withdrawal request.



eprints@whiterose.ac.uk
<https://eprints.whiterose.ac.uk/>

Solvent-Mediated Enhancement of Additive-Controlled Crystallization

Ouassef Nahi, Alexander N. Kulak, Alexander Broad, Yifei Xu, Cedrick O'Shaughnessy, Olivier J.*

*Cayre, Sarah J. Day, Robert Darkins and Fiona C. Meldrum**

1. Materials

CaCl₂·2H₂O, SrCl₂·6H₂O, MnCl₂·4H₂O, MgCl₂·6H₂O, (NH₄)₂CO₃, NaHCO₃, Na₂SO₄, Brilliant Blue R (BBR), Amaranth, Fast Green, Reactive Green 19, aspartic acid and glycine, absolute methanol, ethanol, 1-propanol, 2-propanol and dioxane were purchased from Sigma Aldrich (UK). All solutions were prepared using Milli-Q deionized (DI) water. Glass slide substrates were thoroughly cleaned by soaking in Piranha solution (H₂SO₄ : H₂O₂ – 70 vol% : 30 vol%), washed with DI water followed by ethanol, and dried using N₂(g) stream, prior to use.

2. CaCO₃ mineralization in the presence of soluble additives in pure water and binary solvent mixtures

Calcium carbonate (CaCO₃) was precipitated using the ammonium carbonate diffusion method¹ in the presence of the soluble additives (*i.e.*, ions, amino acids or dye molecules) both in pure aqueous solution and in the presence of varying amount of organic co-solvents (0 – 75 vol%). Glass substrates were deposited at the bottom of a well-plate containing a total volume of 1 mL of solution. Desired amounts of additives were introduced in mineralization medium containing [Ca²⁺] = 10 mM – 500 mM in pure aqueous solutions or in the presence of 5 – 75 vol% of co-solvent (*i.e.*, methanol, ethanol, 1-propanol, 2-propanol or dioxane). Calcification in the presence of the additives was carried out by placing the reaction mixtures inside a sealed desiccator, containing 2 g of (NH₄)₂CO₃, placed in a Petri-dish covered with Parafilm punctured several times with a needle. Mineralization was allowed to proceed overnight (> 12 h). After reaction completion, the substrates supporting the crystals were washed several times with DI water and then ethanol, followed by gentle drying using N₂(g) stream, prior to characterization.

3. Precipitation of MnCO₃ and SrSO₄ in the presence of soluble additives in pure water and binary solvent mixtures

SUPPORTING INFORMATION

Rhodochrosite (MnCO_3) and celestine (SrSO_4) were precipitated by mixing equal volumes of $[\text{Mn}^{2+}] = 2 \text{ mM}$ and $[\text{NaHCO}_3] = 200 \text{ mM}$ and $[\text{Sr}^{2+}] = 4 \text{ mM}$ and $[\text{Na}_2\text{SO}_4] = 20 \text{ mM}$, respectively. Glass substrates were deposited at the bottom of a well-plate containing a total volume of 1 mL of solution. [Reactive Green] = 0.05 mM was introduced in the MnCO_3 and SrSO_4 mineralization solutions in both pure aqueous solutions and in the presence of 10 vol% of ethanol. Mineralization was allowed to proceed overnight (> 12 h). After reaction completions, the substrates supporting the crystals were carefully washed several times with DI water and then ethanol, followed by drying using $\text{N}_2(\text{g})$ stream, prior to characterization.

4. Characterization methods

4.1. Electron Microscopy

Scanning Electron Microscopy (SEM) was carried out using a FEI NanoSEM Nova 450 to image the crystals grown on glass substrates. The samples were mounted on SEM stubs using carbon adhesive discs and were coated with a 4 nm iridium layer, prior to imaging.

Samples for Transmission Electron Microscopy (TEM) were prepared by placing a 10 μL droplet of a solution of BBR (in pure water or in the presence of ethanol) on a TEM grid for 1 min. Excess solution was removed via blotting. Copper TEM grids coated with a carbon film were employed, and these were treated with a plasma glow discharge for 30 sec to create a hydrophilic surface prior to addition of BBR solutions. A thin slice of BBR/calcite composite crystals was prepared using FIB-SEM and transferred to a copper TEM grid using a Kleindiek micromanipulator. TEM analyses were conducted using a FEI Tecnai TF20 FEGTEM with an Oxford Instruments INCA 350 EDX system/80 mm X-Max SDD detector and a Gatan Orius CCD camera operating at 200 kV.

Cryogenic Transmission Electron Microscopy (cryo-TEM) analyses of the early stages of CaCO_3 mineralization in pure water and in the presence of ethanol were carried out by placing a 3 μL droplets of the reaction solutions (after $\approx 30 \text{ min}$) on Quanti-foil TEM grid that were treated with a plasma glow discharge for 40 sec to create a hydrophilic surface. The TEM grids supporting the samples were then

SUPPORTING INFORMATION

blotted and vitrified using an automated vitrification robot (FEI Vitrobot). CryoTEM imaging was carried out under 5 μm defocus on a Thermo Fisher Scientific Titan Krios microscope equipped with a field emission gun operating at 300 kV. Images were recorded on an energy filtered Gatan K2 summit camera using a low electron dose of $5 \text{ e}^- \text{ \AA}^{-2}$ per image.

4.2. Quantification of amount of dye incorporated in calcite

The extent of occlusion of BBR in calcite was quantified using Atomic Absorption Spectroscopy (AAS) in conjunction with UV-Vis spectrophotometry. UV-Vis spectra were recorded using a NanoDrop One/One^C Microvolume UV-Vis spectrophotometer and AAS measurements were performed using a Perkin Elmer Atomic Absorption Spectrometer AAnalyst 400, operating with an air-acetylene flame. The dye/calcite composite crystals were first dissolved overnight in 5 mL of an aqueous solution containing 200 mM EDTA disodium salt and 0.66 M potassium borate buffer (pH 10.5). The amount of dye released was then quantified by recording the absorbance at of the characteristic peaks of the dye molecules and comparing it to the calibration curves (absorbance vs [dye]) obtained from the EDTA buffered solutions. The extent of CaCO_3 in the samples was quantified by AAS that was prior calibrated with Ca standard solutions. The ratios between the [BBR] and the [CaCO_3] contents in each sample provide the precise extents of dye incorporation within calcite.

4.3. Thermogravimetric analysis (TGA)

Thermogravimetric analyses (TGA) were performed from 20 $^\circ\text{C}$ to 850 $^\circ\text{C}$ in air, using a TA-Instruments Q600 operating at 10 $^\circ\text{C min}^{-1}$. The samples were bleached prior to characterization to remove the surface bound organic matter.² Calcination of the pure calcite reference shows an onset of decomposition at 650 $^\circ\text{C}$, giving a weight loss of 44.0 wt% that is ascribed to the release of $\text{CO}_2(\text{g})$, leaving a residue of 56.0 wt% that corresponds to $\text{CaO}(\text{s})$. The levels of incorporation of glycine (Gly) and aspartic acid (Asp) in calcite were determined by measuring the weight losses of the composites below 600 $^\circ\text{C}$, where these are induced by the thermal decomposition of the amino acids in the crystals. Similarly, the levels of incorporation of Reactive Green (RG) incorporated within MnCO_3 and SrSO_4 ,

SUPPORTING INFORMATION

were determined by measuring the weight losses occurring below 300 °C for rhodochrosite (above which manganese oxide forms) and up to 900 °C for celestine. Note that the thermogram of RG alone (Figure S16) shows that < 5 wt.% char residues of the dye remain in the crucible, even after heating at 900 °C. This shows that most of the dye decomposes at elevated temperature and that slightly higher levels of occlusion in calcite are expected. However, the wt% of residual organic matter is consistent for all analyses, and the ratios of additives incorporated in the minerals in pure aqueous solutions and in the presence of various amounts of organic co-solvents are accurate.

4.4. Synchrotron High-Resolution PXRD

High resolution synchrotron powder XRD (HR-PXRD) measurements were performed at beamline ID22 at the European Synchrotron Radiation Facility (ESRF, Grenoble, FRANCE) and beamline I11 at Diamond Light Source (Didcot, UK). Instruments calibrations were performed using a high purity NIST SRM640c Si(111) standards. A wavelength of $0.35449587 \pm 0.00000467 \text{ \AA}$ and $0.826764 \pm 0.000001 \text{ \AA}$ were employed for the analyses of the crystals at the ESRF and Diamond Light Source beamlines, respectively. The powder samples were loaded into 0.5 mm borosilicate glass capillaries and the diffractograms were recorded at room temperature.

The structural parameters were refined by Rietveld refinement using PANalytical X'Pert HighScore Plus software. Lattice distortions (%), microstrain fluctuations (%) and coherence lengths (*i.e.*, crystallite sizes, nm) were derived from the analyses of the whole spectra and line profile analyses were performed for the (104) reflection of calcite. Goodness of fit (GOF) for all analyzed samples were < 8, showing good quality of the fittings.

4.5. Other measurements

Optical micrographs of the specimens were recorded using a Nikon Eclipse LV100 polarizing microscope, equipped with both transmitted and reflected light sources. Fourier transform infrared spectra (FTIR) were acquired over the mid-infrared region ($600 \text{ cm}^{-1} - 2000 \text{ cm}^{-1}$) using a Perkin–Elmer ATR-IR instrument. Individual crystal polymorphs were obtained by Raman spectroscopy, using

SUPPORTING INFORMATION

a Renishaw 2000 Raman Microscope, equipped with a 785 nm diode laser. Turbidimetry was used to probe the effects of the ethanol on the early stages of the CaCO₃ precipitation by monitoring the light absorbed by the samples. Turbidity measurements were carried out over time using a NanoDrop One/One^c Microvolume UV-Vis spectrophotometer by mixing equal volumes of [Ca²⁺] = 20 mM and [NaHCO₃] = 200 mM aqueous solutions in the absence and the presence of ethanol (5 – 75 vol%). The recorded absorbance measurements were converted into transmittance recovery plots using $\text{Transmittance} = 10^{2 \cdot \text{Absorbance}}$.

SUPPORTING INFORMATION

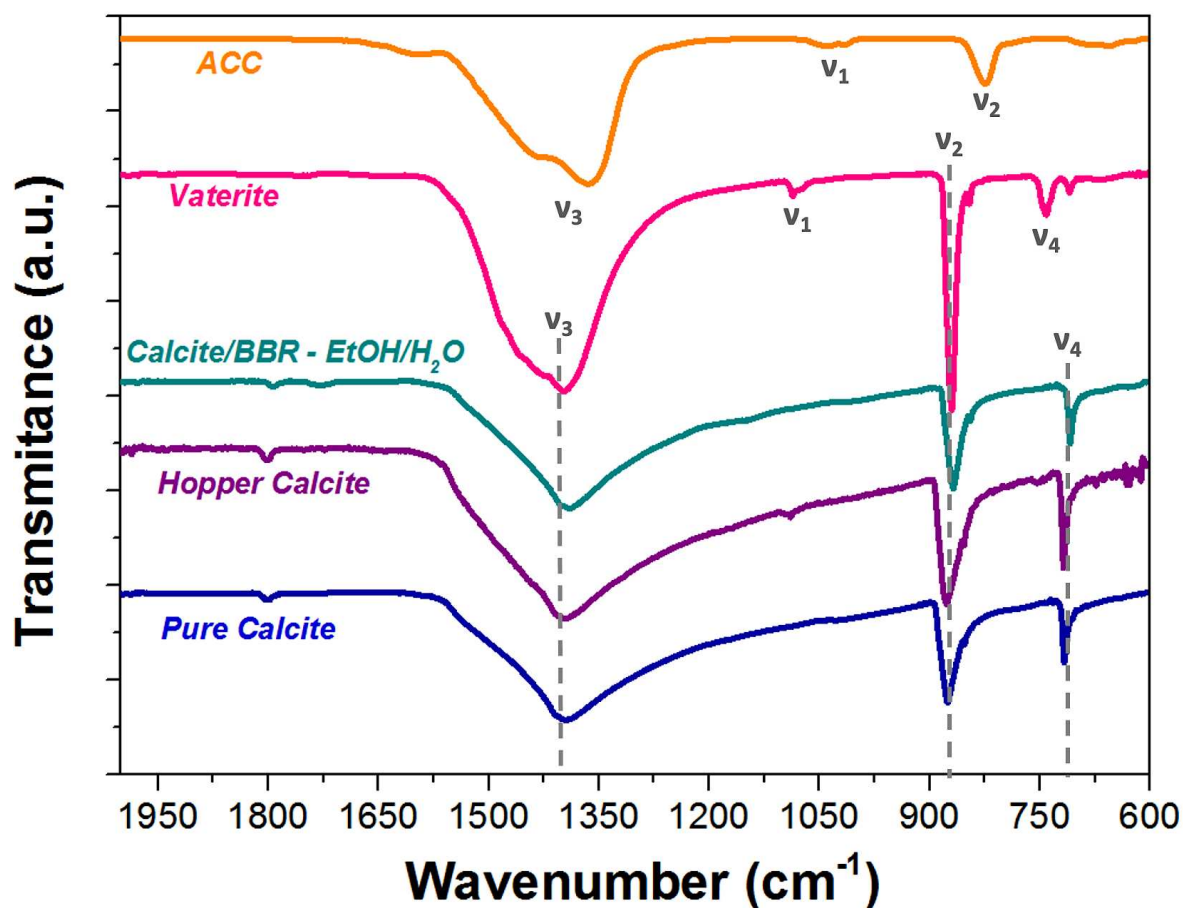


Figure S1. FTIR spectra of ACC (orange), vaterite (pink), pure calcite (blue), hopper calcite (purple) and calcite/BBR hybrid crystals grown in ethanol-water mixtures, showing the characteristic vibrational peaks corresponding to each polymorph: ν_1 (symmetric stretching), ν_2 (out-of-plane CO_3 bending), ν_3 (asymmetric CO_3 stretching) and ν_4 (in-plane CO_3 bending). Only calcite is precipitated in pure water or in the presence of ≤ 25 vol% of ethanol. Hopper calcite crystals are precipitated when the ethanol content is less than 50 vol%, while increasing the amount of ethanol to > 50 vol% considerably stabilizes an ACC precursor phase that eventually recrystallizes into vaterite.

SUPPORTING INFORMATION

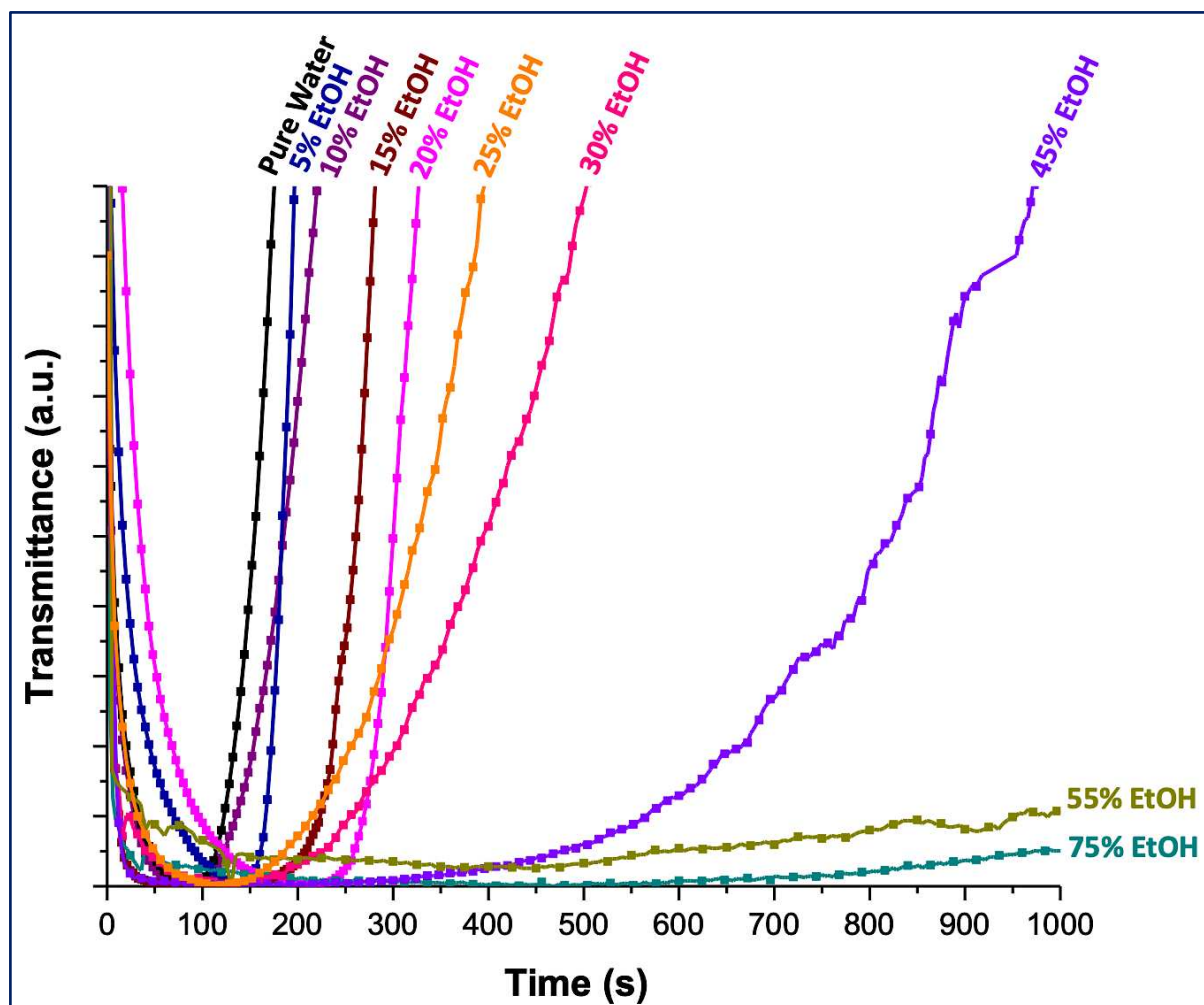


Figure S2. UV-Visible transmittance recovery as a function of time after mixing solutions of 20 mM CaCl_2 and 200 mM NaHCO_3 in pure water and various ethanol/water ratios. Amounts of ethanol ≤ 30 vol% in solution do not significantly alter ACC precipitation and stability, where immediate precipitation of the amorphous phase is observed after mixing the ionic precursors. Dissolution starts after 100 – 250 sec following mixing. In contrast, larger amounts of ethanol in solution (≥ 45 vol%) considerably enhance ACC stability, where transmittance recovery is significantly delayed.

SUPPORTING INFORMATION

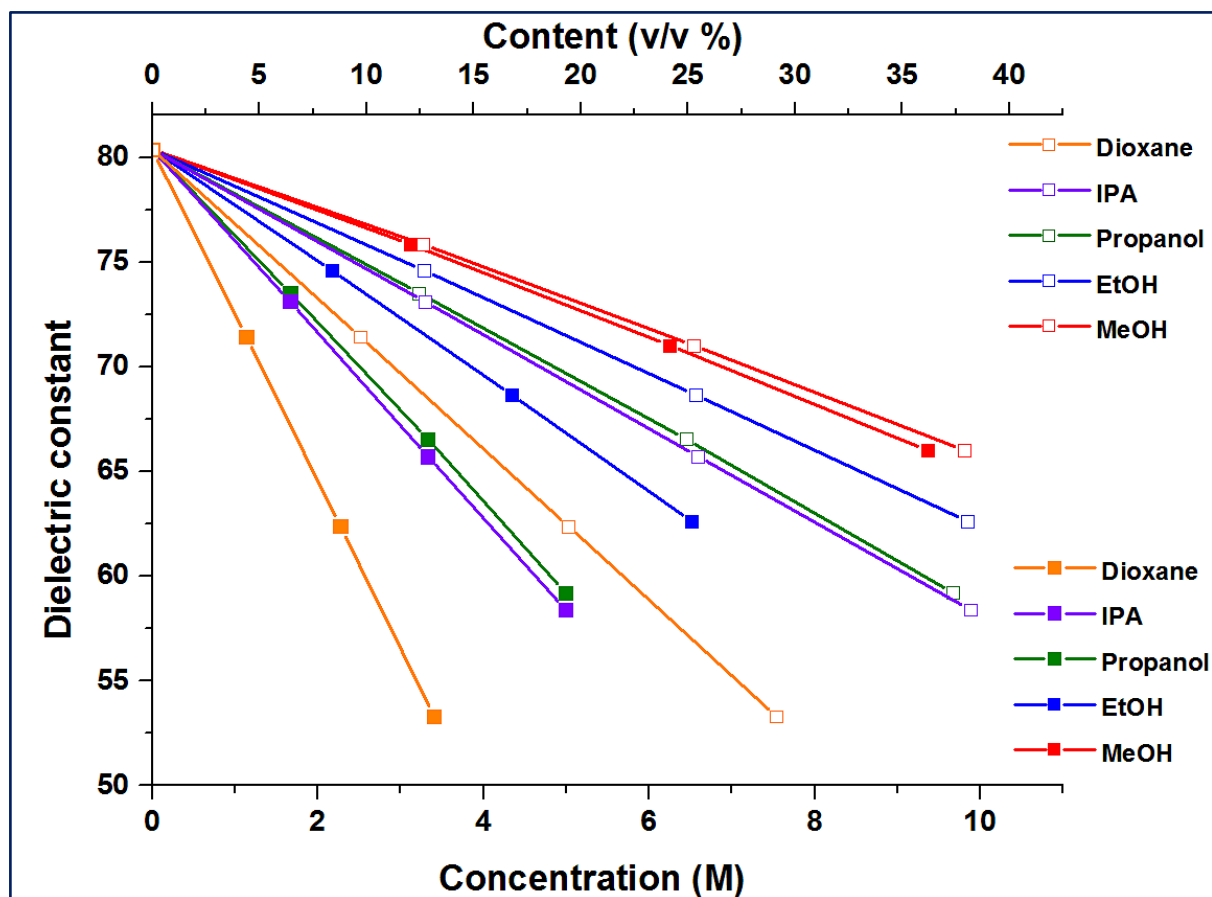


Figure S3. Graph showing the effect of the composition of various binary solvent mixtures on the dielectric constant of the solution at room temperature. The filled and empty squares correspond to the variation of the dielectric constant of the solution as a function of the co-solvent concentration and volume ratio, respectively.^{3,4}

SUPPORTING INFORMATION

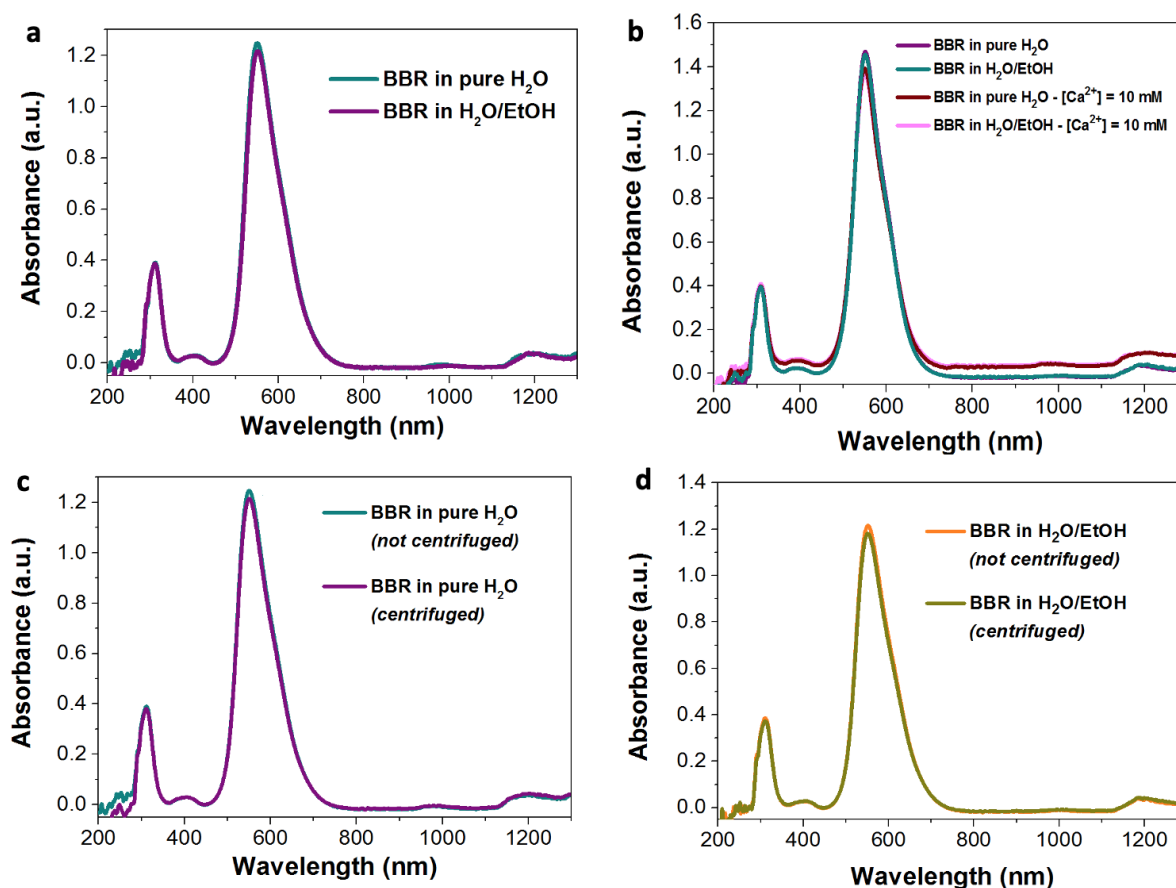


Figure S4. (a-b) UV-Visible-IR spectra of BBR solutions prepared in pure water and 20 vol% ethanol, in the absence and presence of Ca^{2+} ions. No significant changes in the spectra are recorded, which reveals that ethanol does not affect the structure of the dye. (b) The slight decrease in intensity of the absorbance peak at 550 nm is attributed to the complexation of Ca^{2+} ions with the dye. (c-d) UV-Visible-IR spectra of BBR solutions prepared in pure water and in the presence of 15 vol% ethanol before and after centrifugation. The minor decrease in intensity of the absorbance peak at 550 nm is attributed to the removal of dye aggregates in both solutions.

SUPPORTING INFORMATION

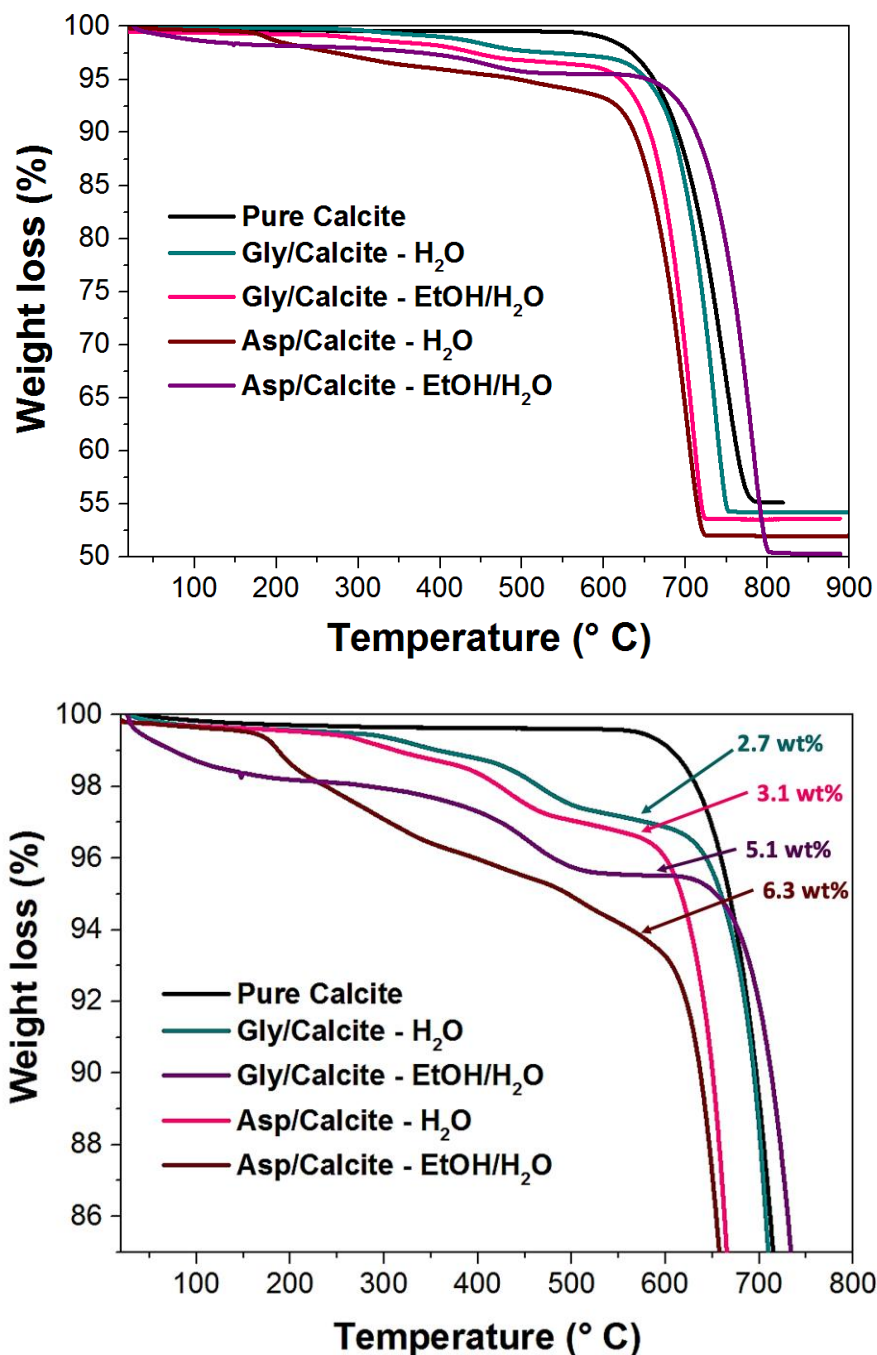


Figure S5. TGA of pure calcite (black), glycine/calcite (blue), aspartic acid/calcite (pink) grown in pure water and glycine/calcite (purple), aspartic acid/calcite (burgundy) grown in the presence of 15 vol% EtOH. The levels of occlusion of glycine (Gly) and aspartic acid (Asp) calcite are determined by the thermal degradations of the amino acids that induce weight losses when the composite crystals are annealed at temperatures below 600 °C. Thermal decomposition of $\text{CaCO}_3(\text{s}) \rightarrow \text{CaO}(\text{s})$ and $\text{CO}_2(\text{g})$ takes place at temperature above 600 °C.

SUPPORTING INFORMATION

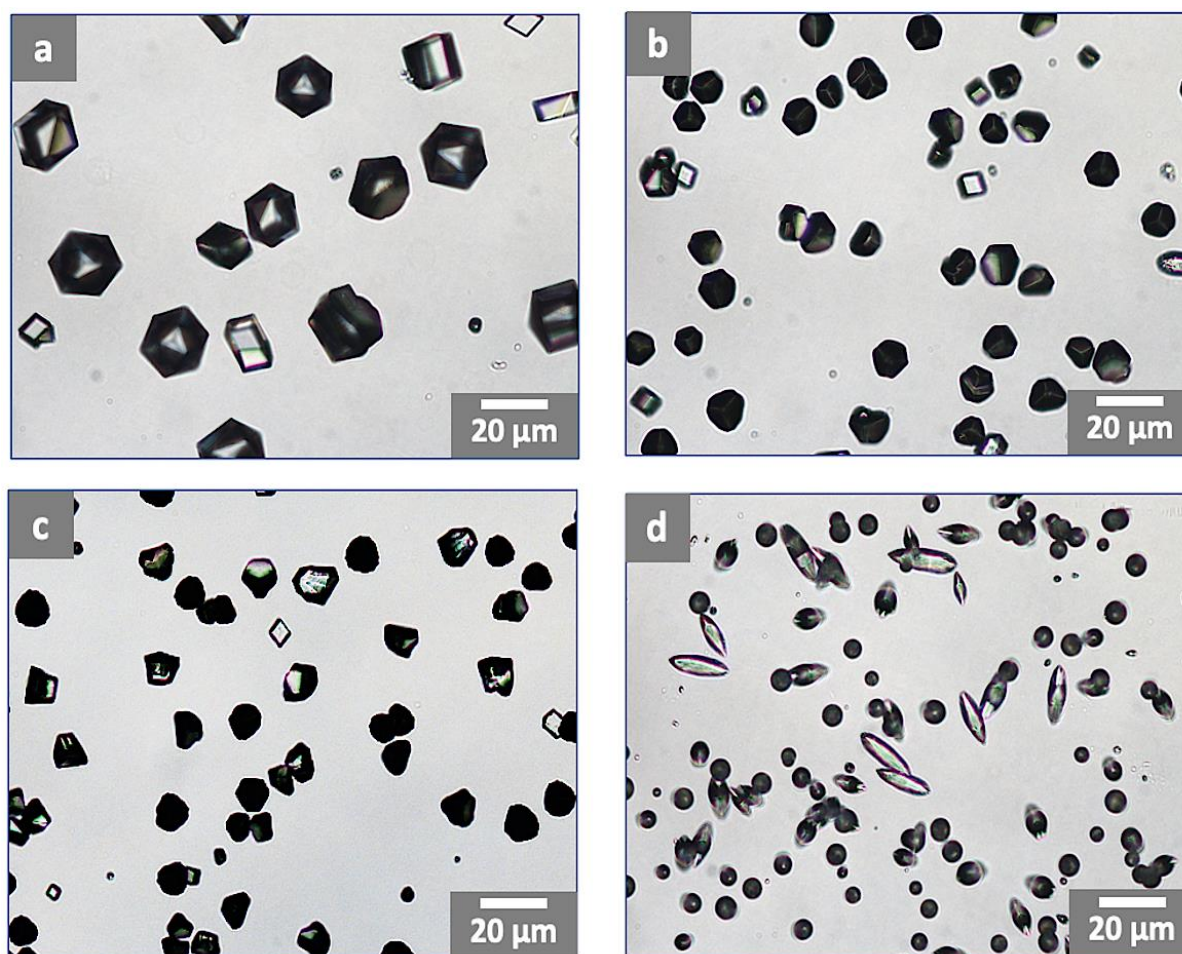


Figure S6. Optical images of calcite precipitated in the presence of $[\text{Ca}^{2+}] = 10 \text{ mM}$ and $[\text{Mg}^{2+}] = 5 \text{ mM}$, in (a) pure water and in the presence of (b) 5 vol%, (c) 10 vol%, and (d) 15 vol% of ethanol. The formation of gradually more elongated calcite crystals is indicative of the increased inclusion of magnesium in calcite.

SUPPORTING INFORMATION

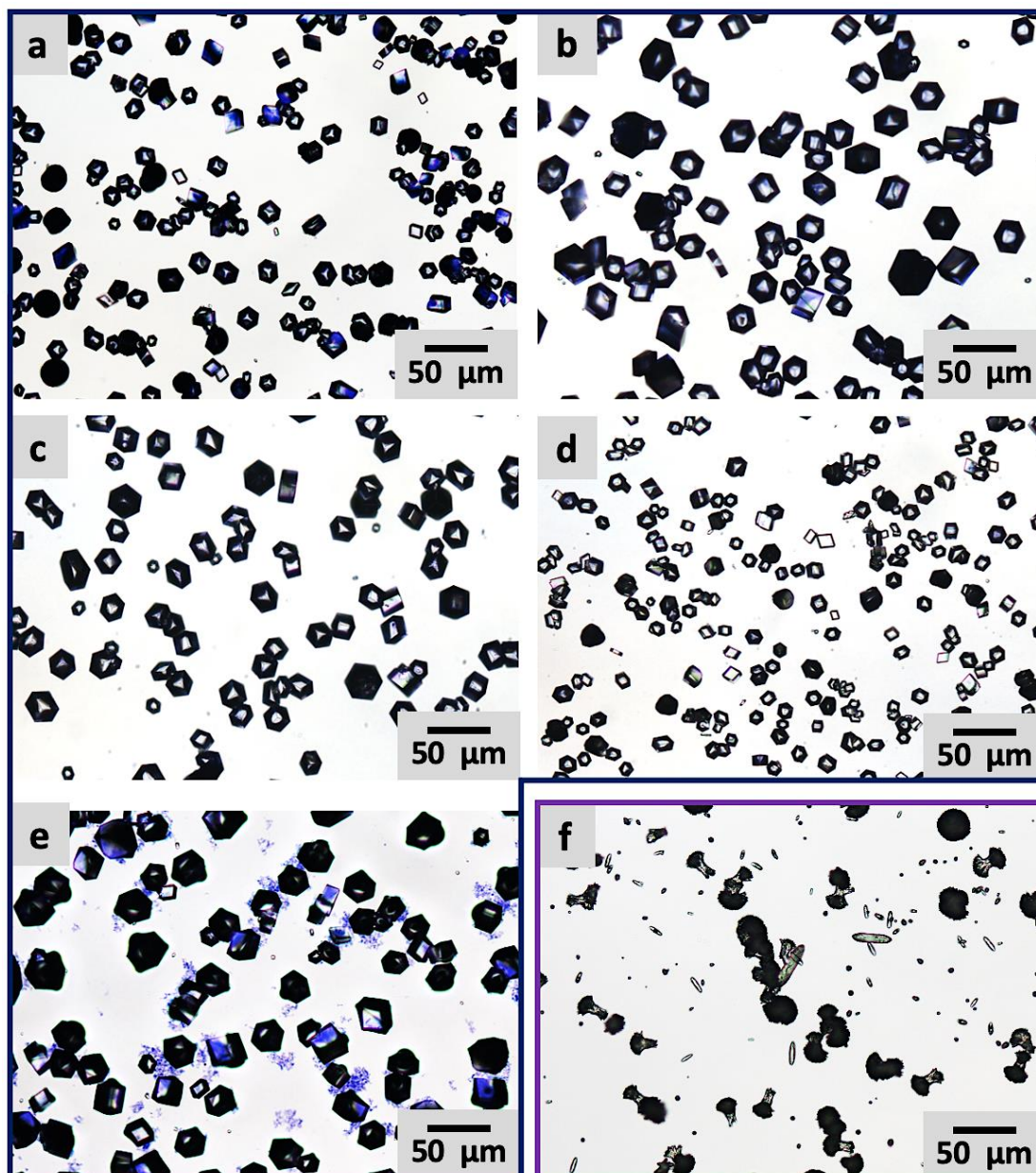


Figure S7. Calcite crystals precipitated in the presence of [BBR] = 0.5 mM and (a) $[\text{Ca}^{2+}] = 50$ mM, (b) $[\text{Ca}^{2+}] = 100$ mM, (c) $[\text{Ca}^{2+}] = 200$ mM, (d) $[\text{Ca}^{2+}] = 500$ mM. An increase of the supersaturation failed to enhance the morphology changes and dye incorporation, where only pale blue calcite rhombs precipitated. (e) Crystallization solution showing calcite crystals obtained from solutions containing [BBR] = 0.2 mM and $[\text{Ca}^{2+}] = 50$ mM. Aggregates of the dye molecules are clearly visible in the crystallization solution. (f) Mixtures of elongated calcite and metastable aragonite polycrystals precipitated from $[\text{Ca}^{2+}] = 20$ mM and $[\text{Mg}^{+}] = 25$ mM.

SUPPORTING INFORMATION

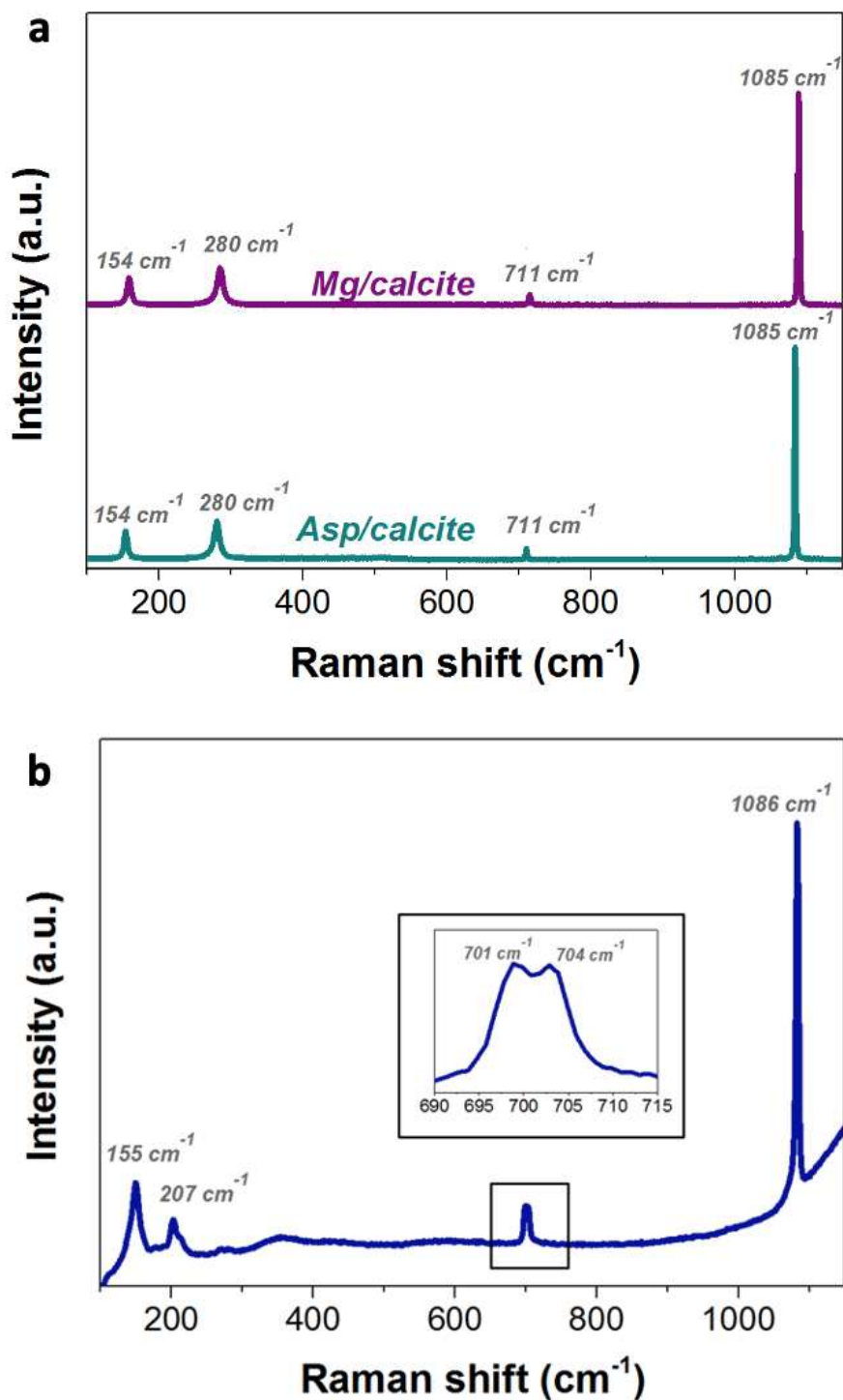


Figure S8. (a) Raman spectra of the CaCO_3 crystals precipitated in the presence of [aspartic acid] = 75 mM and $[\text{Ca}^{2+}] = 20$ mM (cyan), and $[\text{Mg}^{2+}] = 20$ mM and $[\text{Ca}^{2+}] = 10$ mM (purple), showing the characteristic peaks of calcite. (b) Raman spectra of aragonite crystals precipitated in the presence of $[\text{Mg}^{2+}] = 50$ mM and $[\text{Ca}^{2+}] = 10$ mM.

SUPPORTING INFORMATION

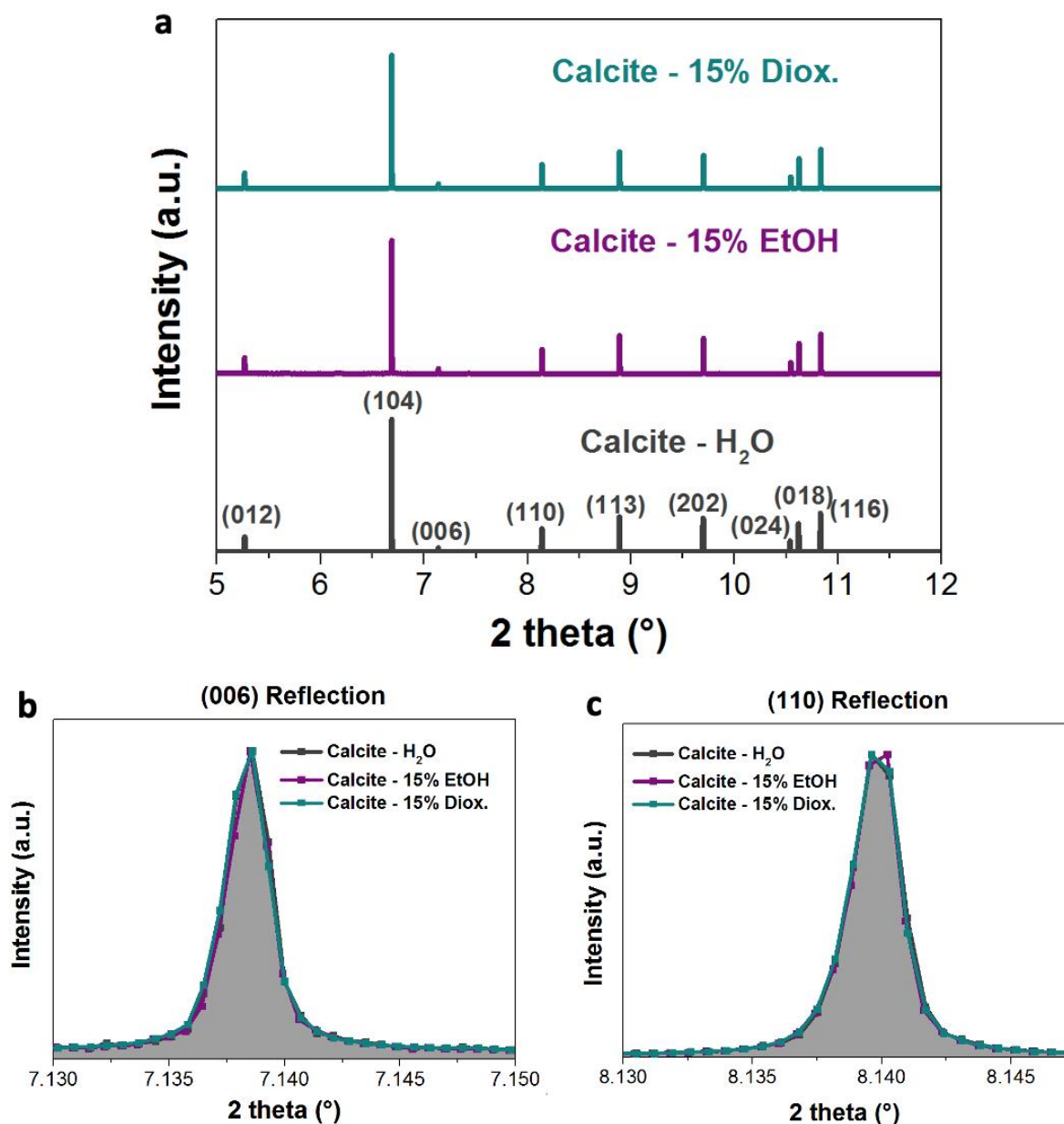


Figure S9. (a) HR-PXRD diffractograms ($\lambda = 0.35449587 \text{ \AA}$) of calcite crystals grown in pure water (dark grey), and in the presence of 15 vol% of ethanol (purple) and dioxane (cyan). (b) HR-PXRD patterns of the (006) and (110) reflections of calcite grown in various solvent mixtures, showing no change in the position, shape and broadening of the peaks. This shows that organic solvents (< 15 vol%) do not affect the microstructure of the calcite crystals.

SUPPORTING INFORMATION

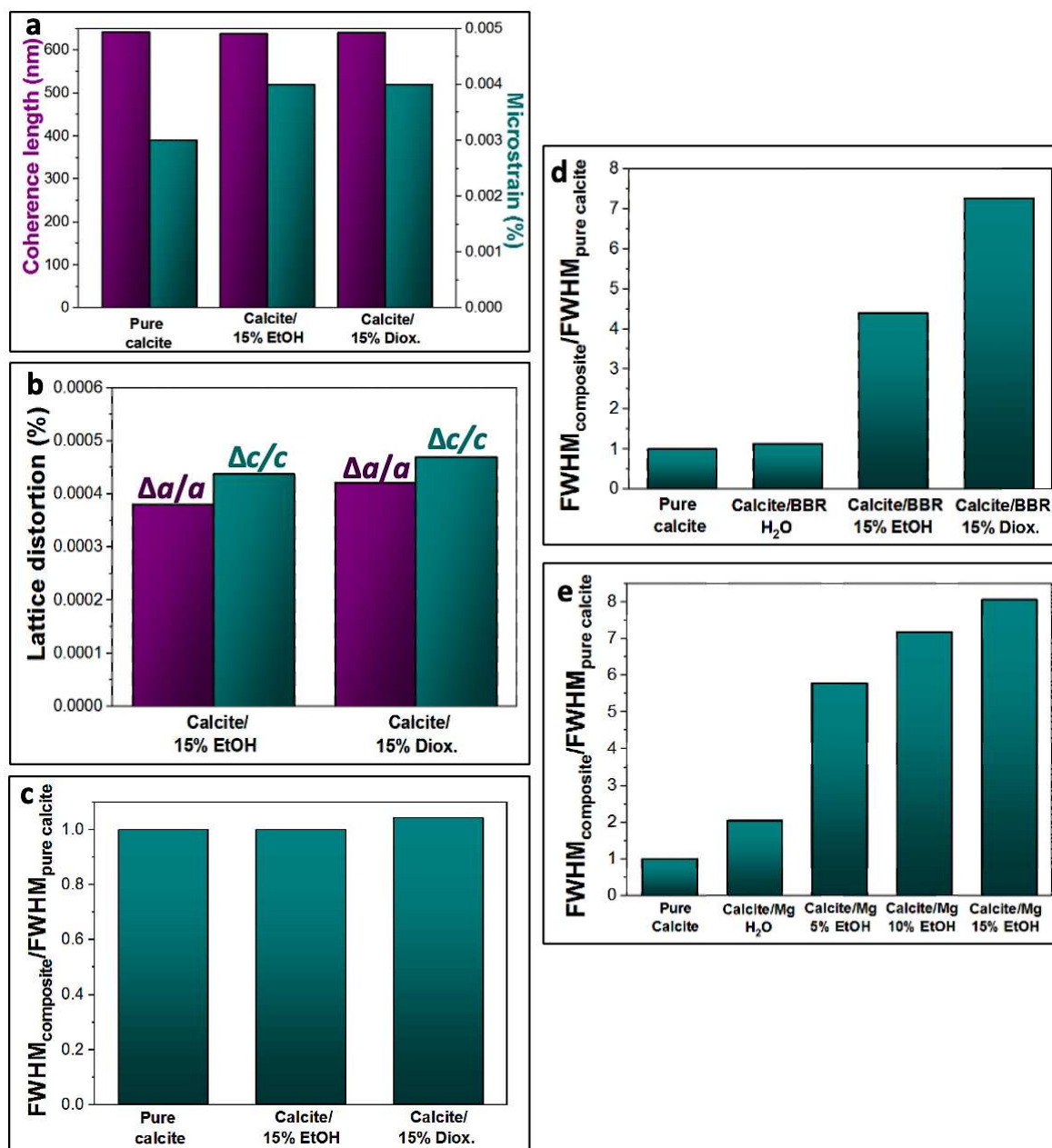


Figure S10. (a) Coherence lengths and microstrain fluctuations, (b) lattice distortions along the *a*-axis and *c*-axis and (c) full-width at half maximum (FWHM) of calcite grown in pure water, and in the presence of 15 vol% of ethanol and dioxane in the mineralization solution. (d) FWHM of pure calcite, and BBR/calcite and (e) Mg/calcite composites, grown in pure water and ethanol/water mixtures.

SUPPORTING INFORMATION

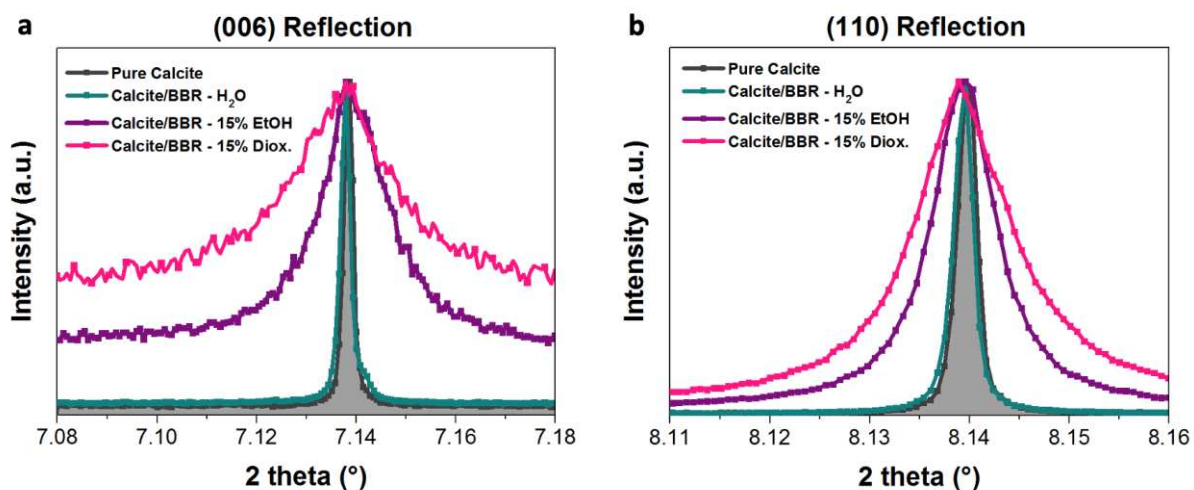


Figure S11. (a-b) HR-PXRD diffractograms ($\lambda = 0.35449587 \text{ \AA}$) of the (006) and (110) reflections of pure calcite crystals (dark grey), and BBR/calcite composites grown in pure water (cyan), and in the presence of 15 vol% ethanol (purple) and in dioxane (pink). The high levels of incorporation of dye in calcite achieved in solvent mixtures mainly generate a significant broadening of the diffraction peaks, while only minor peak shifts are recorded.

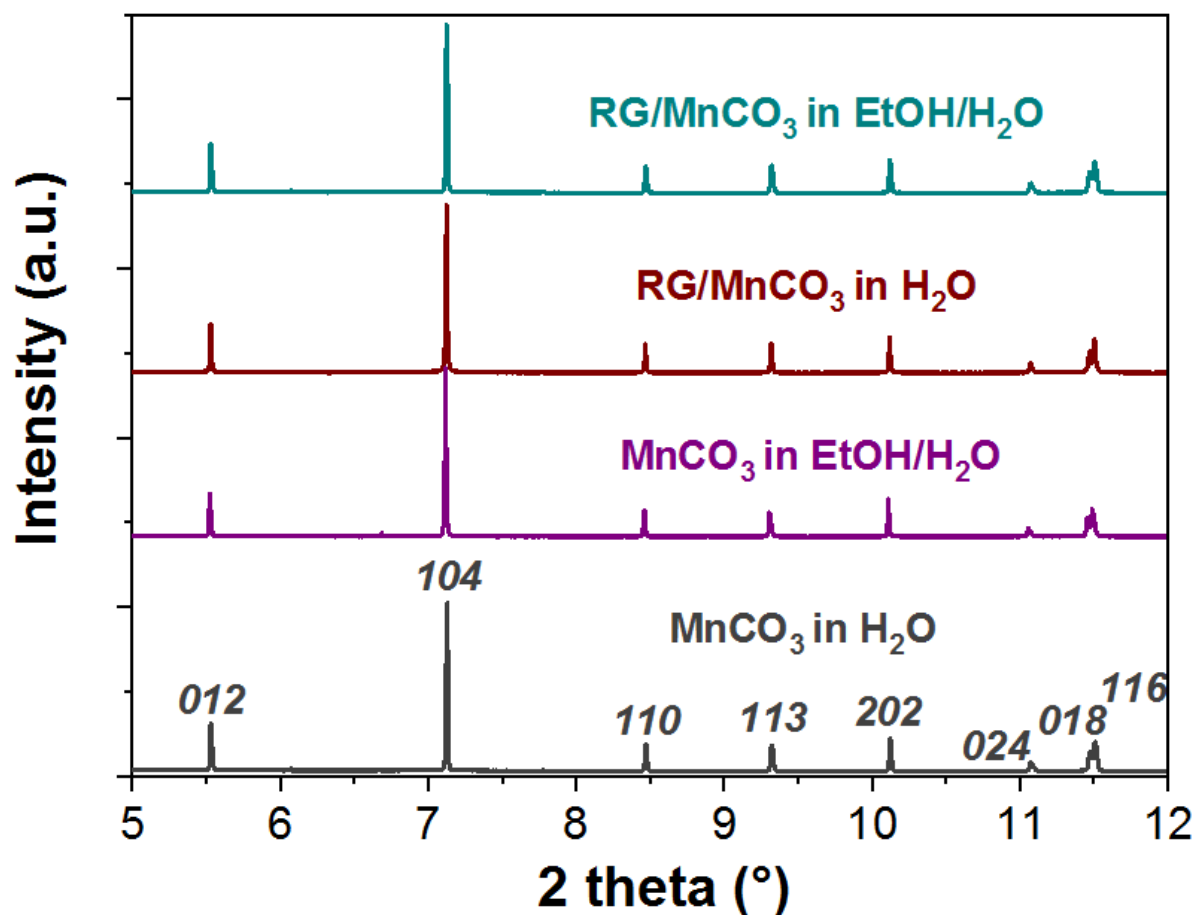


Figure S12. HR-PXRD diffractograms ($\lambda = 0.35449587 \text{ \AA}$) of pure MnCO₃ crystals grown in pure water (dark grey), pure MnCO₃ crystals grown in the presence of 10 vol% of ethanol (purple), Reactive Green/MnCO₃ composites (RG/MnCO₃) precipitated in pure water (dark red), and Reactive Green/MnCO₃ composites (RG/MnCO₃) precipitated in the presence of 10 vol% of ethanol (light blue). In all cases the diffraction peaks correspond to rhodochrosite.

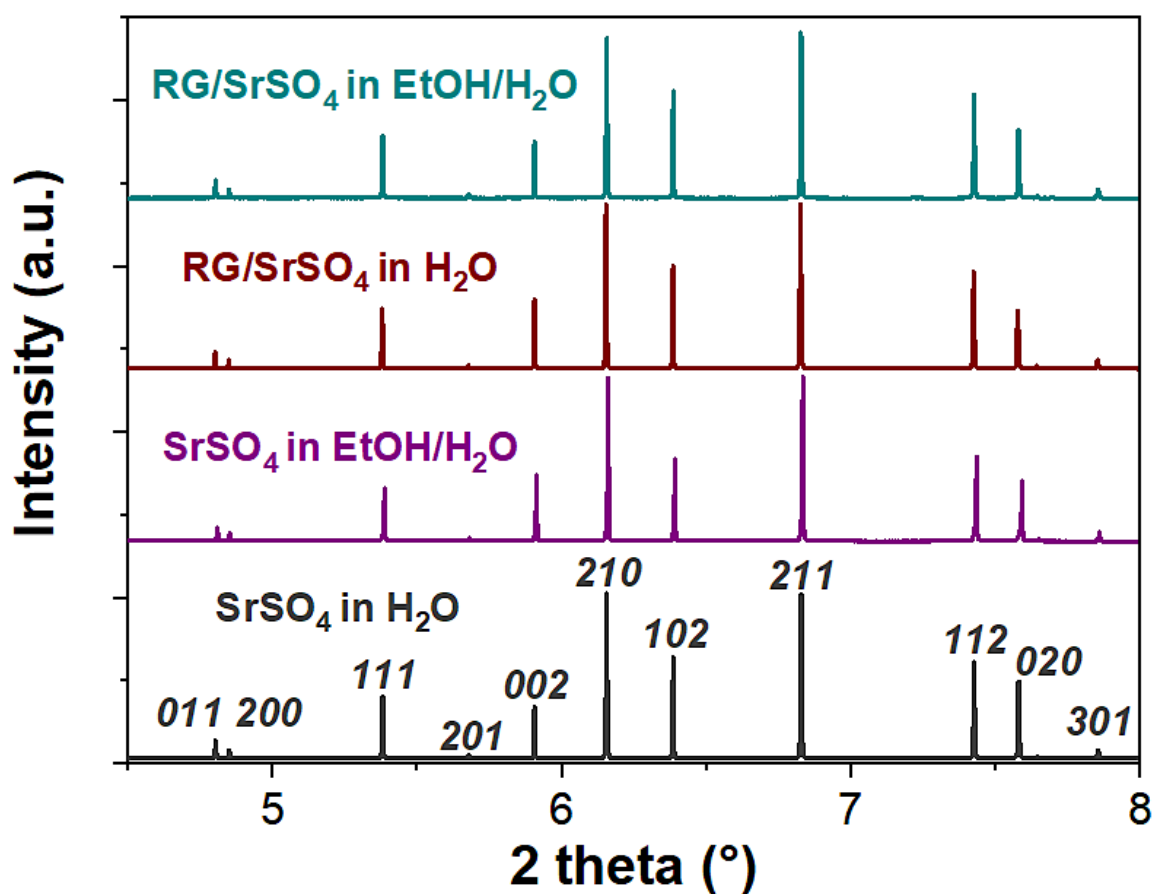


Figure S13. HR-PXRD diffractograms ($\lambda = 0.35449587 \text{ \AA}$) of pure SrSO₄ crystals grown in pure water (dark grey), pure SrSO₄ crystals grown in the presence of 10 vol% of ethanol (purple), Reactive Green/SrSO₄ composites (RG/SrSO₄) precipitated in pure water (dark red), and Reactive Green/SrSO₄ composites (RG/SrSO₄) precipitated in the presence of 10 vol% of ethanol (light blue). In all cases the diffraction peaks correspond to celestine.

SUPPORTING INFORMATION

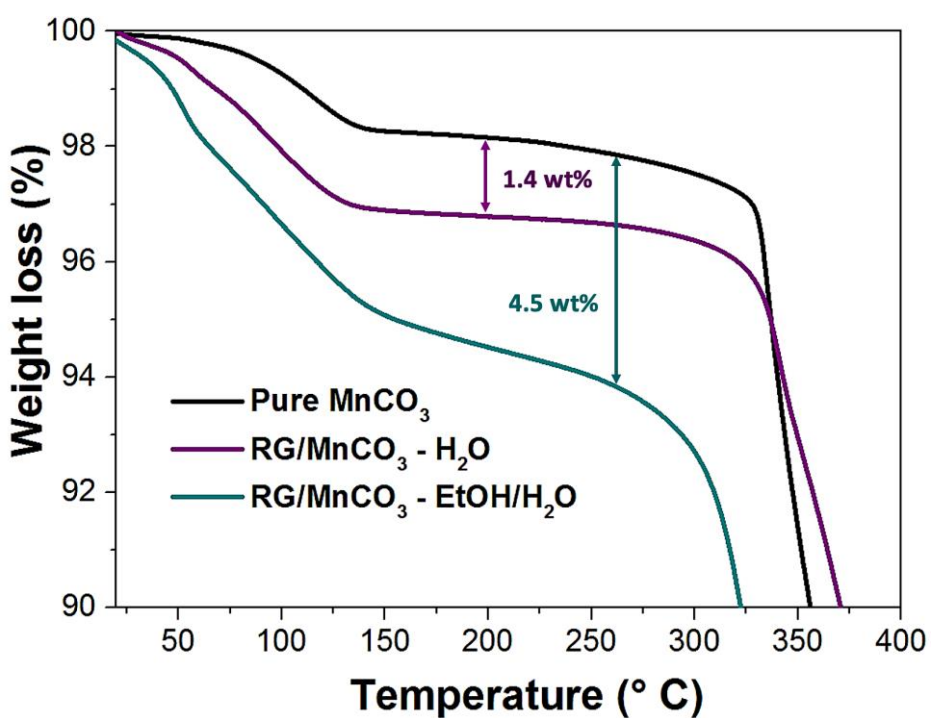
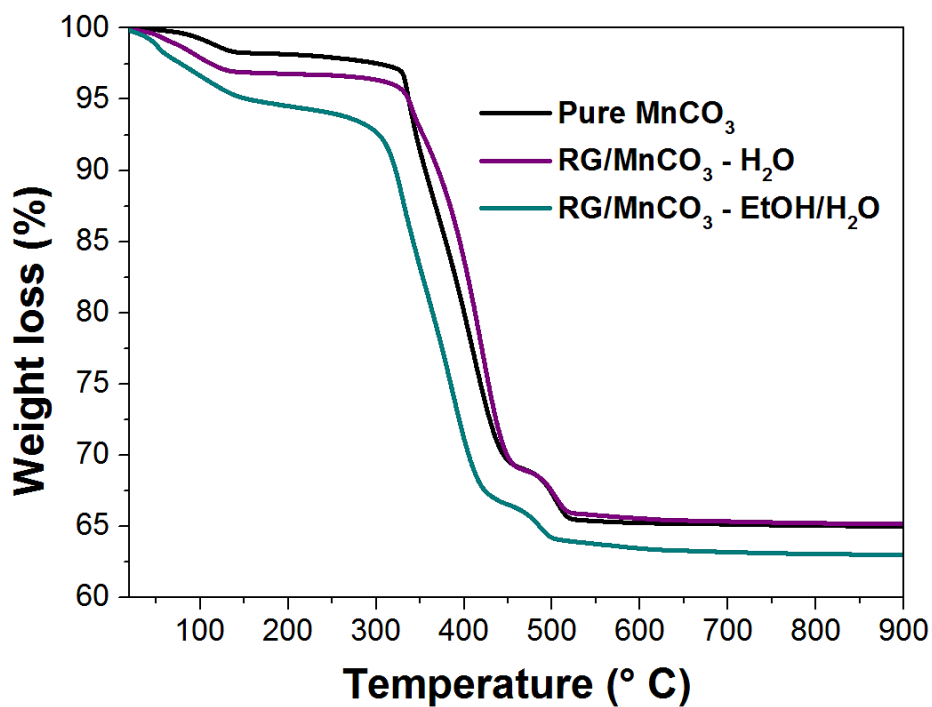


Figure S14. TGA of pure MnCO₃ (black), Reactive Green/MnCO₃ (RG/MnCO₃ – purple) grown in pure water and Reactive Green/MnCO₃ (RG/MnCO₃ – blue) grown in the presence of 10 vol% of ethanol in solution. The levels of dye incorporation in rhodochrosite are determined by the weight losses occurring below 300 °C. Higher annealing temperatures form manganese oxide.

SUPPORTING INFORMATION

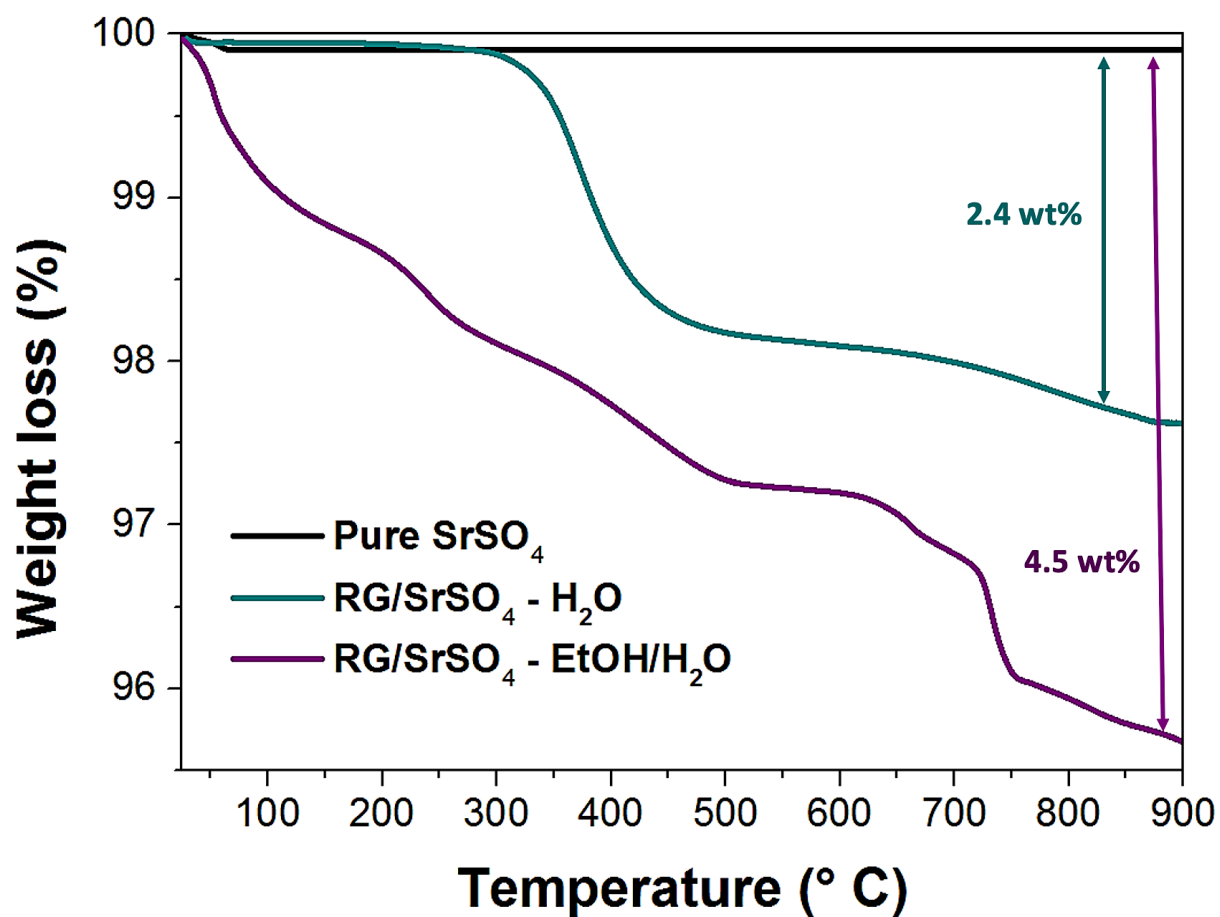


Figure S15. TGA of pure SrSO₄ (black), Reactive Green/SrSO₄ (RG/SrSO₄– blue) grown in pure water and Reactive Green/SrSO₄ (RG/SrSO₄– purple) grown in the presence of 10 vol% of ethanol in solution. The levels of dye incorporation in celestine are determined by the weight losses recorded between room temperature and 900 °C. No weight loss was recorded for pure SrSO₄.

SUPPORTING INFORMATION

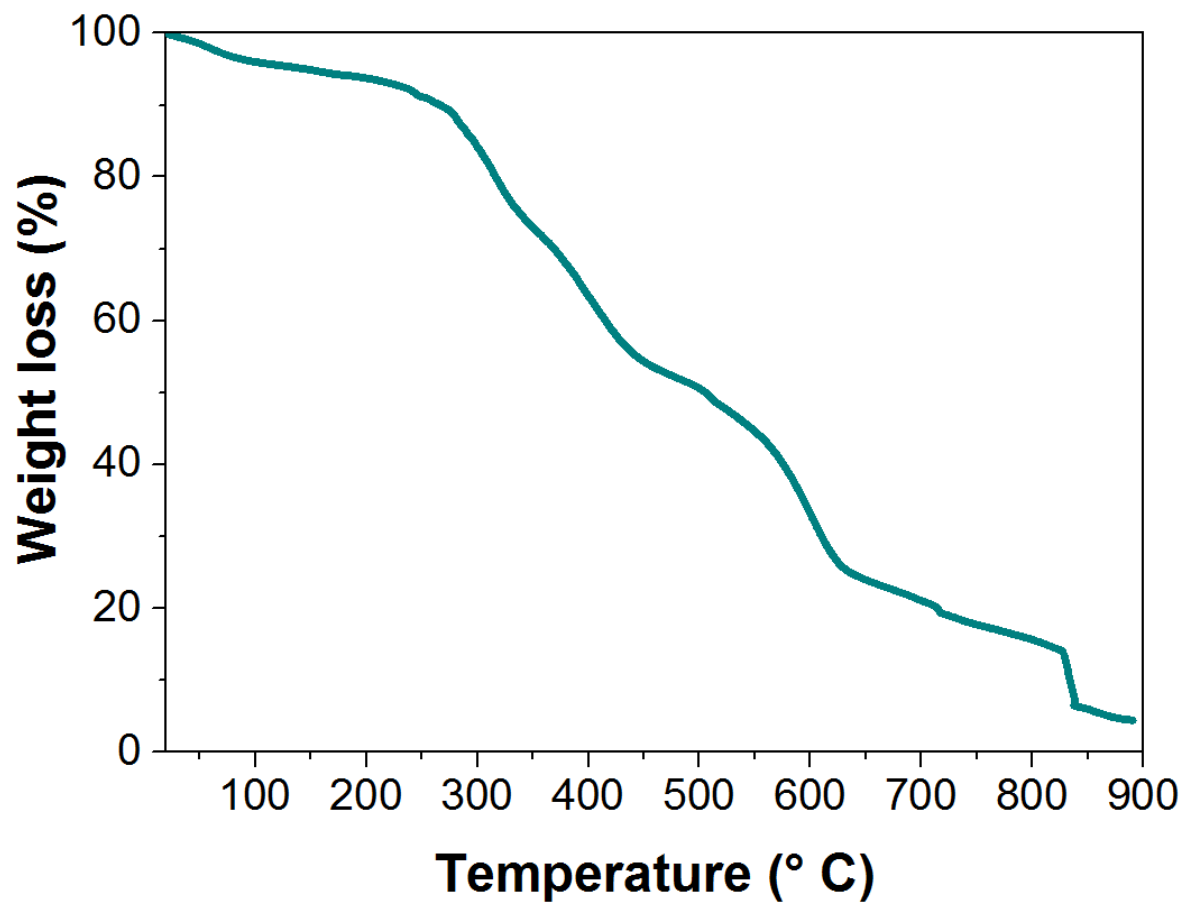
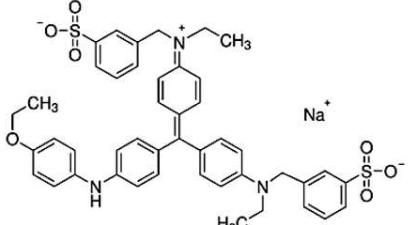
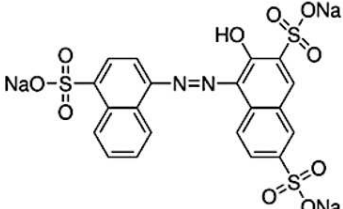
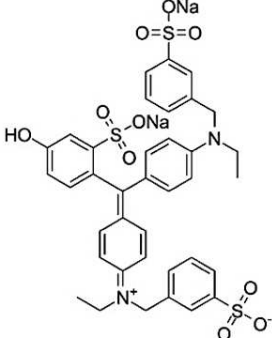
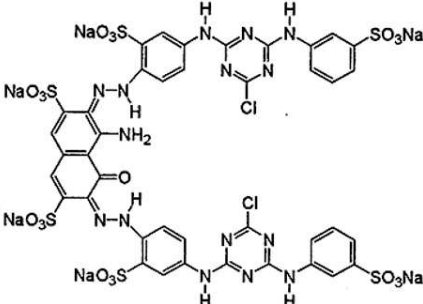


Figure S16. TGA of Reactive Green dye alone showing that < 5 wt% of dye remains in the crucible after annealing at 900 °C.

SUPPORTING INFORMATION

Table S1. Structures and colors of the dye molecules used as additives.

Dye name	Dye structure	Color in solution
Brilliant Blue R (BBR)		Blue
Amaranth		Red
Fast Green		Blue
Reactive Green		Blue/Green

REFERENCES

- (1) Ihli, J.; Bots, P.; Kulak, A.; Benning, L. G.; Meldrum, F. C., Elucidating Mechanisms of Diffusion-Based Calcium Carbonate Synthesis Leads to Controlled Mesocrystal Formation. *Adv. Funct. Mater.* **2013**, 23, (15), 1965-1973.
- (2) Penkman, K. E.; Kaufman, D. S.; Maddy, D.; Collins, M. J., Closed-system behaviour of the intra-crystalline fraction of amino acids in mollusc shells. *Quat. Geochronol.* **2008**, 3, (1-2), 2-25.
- (3) Akerlof, G.; Short, O. A., The Dielectric Constant of Dioxane—Water Mixtures between 0 and 80°. *J. Am. Chem. Soc.* **1936**, 58, (7), 1241-1243.
- (4) Akerlof, G., Dielectric constants of some organic solvent-water mixtures at various temperatures. *J. Am. Chem. Soc.* **1932**, 54, (11), 4125-4139.